

# On the Joint Probability Density Function for the Autocorrelation Estimates in Ultrasound Color Flow Imaging

Hans Torp, *Member, IEEE*, Kjell Kristoffersen, and Bjørn A. J. Angelsen, *Senior Member, IEEE*

**Abstract**—Autocorrelation estimates of the Doppler signal with zero and unity lag are commonly used for color coding algorithm in 2-D color flow imaging. Signal power, center frequency, and bandwidth are derived from these two autocorrelation estimates, and combined in a color coding scheme. In this paper computer simulations show that the joint probability density function (PDF) for the autocorrelation estimates has a form which differs significantly from a Gaussian distribution. However, the PDF for the *normalized* autocorrelation estimates is shown to have a form closer to a Gaussian distribution, which means that the first- and second-order moments gives an adequate statistical description of the set of estimators. Analytical approximations for the first- and second-order moments in the joint PDF for the normalized autocorrelation estimates of all lags are derived, and the expressions are verified by computer simulations. Using this results, an expression for the probability density function of the correlation angle estimate is derived, showing a close fit to simulation results. Numerical results show that the performance of the correlation angle estimate can be improved significantly by applying spatial averaging to the autocorrelation estimates.

## NOMENCLATURE

$R(n, m)$	Autocorrelation function for the Doppler signal with lag $n$ in radial direction, and lag $m$ in temporal direction.
$\mathbf{R}(n, m)$	Autocorrelation <i>estimate</i> of $R(n, m)$ .
$\phi(n, m)$	Phase of the complex autocorrelation estimate $\mathbf{R}(n, m)$ .
$\rho(n, m) = \frac{R(n, m)}{R(0, 0)}$	Normalized autocorrelation function.
$\boldsymbol{\rho}(n, m) = \frac{\mathbf{R}(n, m)}{\mathbf{R}(0, 0)}$	Normalized autocorrelation function estimate.
$C_*(n_1, m_1, n_2, m_2)$	Covariance between $\mathbf{R}(n_1, m_1)^*$ and $\mathbf{R}(n_2, m_2)$ .
$C(n_1, m_1, n_2, m_2)$	Covariance between $\mathbf{R}(n_1, m_1)$ and $\mathbf{R}(n_2, m_2)$ .

Manuscript received July 18, 1994; accepted May 1, 1995. This work was supported by the Norwegian Research Council.

H. Torp and B. A. J. Angelsen are with the Department of Biomedical Engineering, University of Trondheim, N-7005 Trondheim, Norway.

K. Kristoffersen is with Vingmed Sound Research Department, N-1324 Lysaker, Norway.

IEEE Log Number 9413341.

## I. INTRODUCTION

ULTRASOUND Doppler signals from blood can be modeled as a zero mean, complex Gaussian process which is characterized by its complex valued autocorrelation function [1], [2]. By estimating the autocorrelation function of the process, the three parameters signal power, bandwidth, and center frequency can be deduced and used to characterize the blood flow [3]. The statistical properties of the autocorrelation estimates have previously been studied to some detail. Analytical expressions for the second-order moments of the autocorrelation estimates can be found in [4], [5] and these results are generalized to 2-D (range-time) Doppler data in [6]. Bias and variance of mean frequency and bandwidth estimators have been determined from these results under the assumption of low fractional variance and strong filtering [6]. In color flow imaging a combination of signal power, center frequency and/or bandwidth are combined in a color code for display. Usually, the signal power is compared to a threshold to reject noise in the image, but color schemes where the signal power modulates the color intensity or hue is also used. The latter types include "power-mode," where only the signal power determines the color, as well as color schemes where the center frequency determines the hue, and the power determines the brightness [6], [7]. In designing optimum color schemes, the statistical properties of each individual signal parameter as well as the statistical dependency between the parameters should be taken into account. This information is contained in the joint probability density distribution (PDF) for the set of parameters.

Both the center frequency and the bandwidth estimate are nonlinear mappings of the complex autocorrelation estimates, which makes it difficult to deduce analytical expressions for the joint PDF. However, the composite mapping from the autocorrelation estimates into the three dimensional color-space (red, green, and blue) can be optimized directly, without first calculating the center frequency and bandwidth. In the most general formulation, color flow imaging is a mapping from the set of autocorrelation estimates into color-space. If the joint PDF is known for the different flow situations, a mapping which gives maximum color contrast can be constructed. Practical use of this is difficult to achieve without a parametric model for the PDF, and in this paper the set of autocorrelation estimates is adapted to a multidimensional Gaussian distribution.

Second-order moments for the set of autocorrelation estimates with arbitrary lags in radial and temporal direction has been treated in an earlier paper [6]. In this paper computer simulations show that the joint PDF for the autocorrelation estimates has a form which differs significantly from a Gaussian distribution. By normalizing the autocorrelation estimates with the signal power estimate, the PDF shows a better fit to a Gaussian distribution, which is demonstrated by computer simulations in Section II. In Section III, approximate analytical expressions for the first- and second-order moments for the normalized correlation estimates are derived. In Section IV the probability density function for the correlation angle estimator is studied; analytical expressions are compared to results from computer simulations.

## II. THE JOINT PROBABILITY DENSITY FUNCTION FOR THE AUTOCORRELATION ESTIMATES

In this section, a 1-D discrete time complex Gaussian process  $x(n)$  is considered. The autocorrelation estimate with lag  $m$  is obtained by averaging the product terms of the signal

$$\mathbf{R}(m) = \sum_{k=0}^{N-1} x^*(n+k)x(n+k+m). \quad (1)$$

To evaluate the shape of the joint PDF for  $\{\mathbf{R}(m)\}_{m=0,1,\dots}$ , computer simulations have been performed. The output of a correlation estimator with lag  $m = 0$ , and  $m = 1$  is plotted in scatter diagrams for simulated signals with different power spectra. The signal was obtained by generating a complex white noise sequence with a random number generator, and then shaping the power spectrum by filtering with a complex FIR band-pass filter, with variable bandwidth and center frequency. A triangular envelope was selected for the filter impulse response, which corresponds to a rectangular burst transmitted pulse, and a receiver filter with rectangular impulse response matched to the transmitted pulse. Independent white noise was added to get a signal with a pre-determined signal to noise ratio, and the resulting signal was high-pass filtered with a cutoff frequency of 0.65 radians to simulate the effect of a typical wall motion filter.

Since  $\mathbf{R}(0)$  is real valued, the estimators form a 3-D real valued vector  $(x, y, z) = [\text{Re}\{\mathbf{R}(1)\}, \text{Im}\{\mathbf{R}(1)\}, \mathbf{R}(0)]$ . To visualize the 3-D probability density function, scatter plots generated from computer simulations are shown in two different 2-D projections. A necessary (but not sufficient) condition for the three dimensional vector to be Gaussian is that both projections are Gaussian distributed. The results from the simulations are shown in Fig. 1 for two different projections of the three dimensional vector  $(x, y, z)$ ,  $x = \text{Re}\{\mathbf{R}(1)\}$ ,  $y = \text{Im}\{\mathbf{R}(1)\}$ ,  $z = \mathbf{R}(0)$ . At the top the  $y/z$ -plane is shown, and at the bottom the  $y/x$ -plane is shown. Scatter plots from three signals with different center frequencies and bandwidths were included in the same diagram.

The scatter plots for the two narrow-band signals, both with fractional rms bandwidth  $B/\omega_1 = 10\%$ , show that the PDF has a form which is highly different from a Gaussian PDF. In the complex  $\mathbf{R}(1)$  plane, the PDF shows an asymmetric,

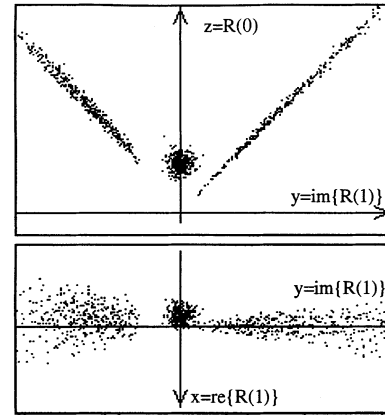


Fig. 1. Scatter diagram of the autocorrelation estimator with lag  $m = 0$  and  $m = 1$  for three different signals. To the right, signal with center frequency  $\omega_1 = 0.5\pi$ ,  $B = 0.05\pi$  to the left, signal with  $\omega_1 = 1.5\pi$ ,  $B = 0.15\pi$ , and in the middle, high-pass filtered white noise.

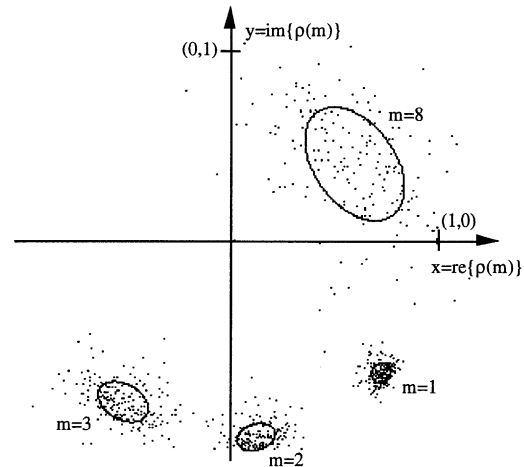


Fig. 2. Scatter diagram for the normalized correlation estimator  $\rho(m)$  with lag  $m = 1, 2, 3$ , and  $8$ . The ellipses indicate the form of a Gaussian approximation of the PDF.

parabolic shape, with a long tail reaching beyond the limits of the plotting diagram.

Another observation in Fig. 1 is the high correlation between  $\mathbf{R}(0)$  and  $\text{Im}\{\mathbf{R}(1)\}$ . This indicates that the quotient  $\rho(m) = \mathbf{R}(m)/\mathbf{R}(0)$  could have a lower fractional variance than the numerator and the denominator separately. This is demonstrated in Fig. 2 where the scatter diagram for the normalized autocorrelation function  $\rho(m)$ ,  $m = 1, 2, 3$ , and  $8$  is shown for a signal with center frequency  $\omega_1 = 0.7$  radians, fractional rms bandwidth of 10%, and signal to noise ratio 20 dB. The PDF of  $\rho(m)$  is seen to be much closer to a Gaussian form than the PDF of  $\mathbf{R}(m)$ . The mean and variances in  $x$  and  $y$  direction as well as the correlation coefficient is estimated from the simulated data, and the result is plotted as ellipses which correspond to the contour  $e^{-1/2}$  for the corresponding Gaussian PDF. This is described in more details in Section III, (5).

The next step is to look at the joint probability density for  $\rho(1)$  and  $\mathbf{R}(0)$ , and to study the effect of adding broad band noise. Since the noise is independent of the signal, the

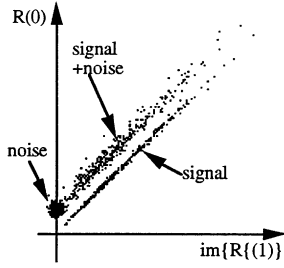


Fig. 3. The effect of adding noise to a narrow band signal, on the estimate of  $\mathbf{R}(0)$  and  $\mathbf{R}(1)$ . Scatter diagram of  $\mathbf{R}(1)$  against  $\mathbf{R}(0)$  for noise only, signal only, and signal in noise. Signal to noise ratio is 3 dB.

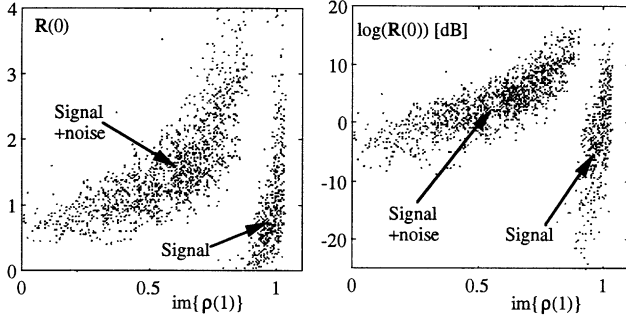


Fig. 4. Scatter diagram of  $\rho(1)$  against  $\mathbf{R}(0)$  to the left, and  $\rho(1)$  against  $\log\{\mathbf{R}(0)\}$  to the right for signal only, and signal in noise.

correlation estimate  $\mathbf{R}(m)$  is a sum of the estimate of the signal alone and the noise alone, plus some product terms between signal and noise, which have zero mean value. The estimator will then be a sum of two independent random variables (neglecting the product terms), and the PDF for signal in noise equals the convolution of the PDF's for the two random variables. This is demonstrated in Fig. 3, left panel, where  $\text{Im}\{\mathbf{R}(1)\}$  is plotted against  $\mathbf{R}(0)$  for signal only, noise only, and signal plus noise. The PDF for the signal only, is concentrated around the line of identity, and after convolution with the circular shaped PDF for the noise, the result is a translation upwards, and a broadening around the line of identity which equals the diameter of the PDF for noise. The upwards shift from the line of identity in the PDF, introduces a negative bias in the normalized autocorrelation estimate  $\rho(1) = \mathbf{R}(1)/\mathbf{R}(0)$ , which increases with decreasing  $\mathbf{R}(1)$ . This leads to a significant correlation between the estimate of  $\rho(1)$ , and  $\mathbf{R}(0)$ , and the joint PDF for  $\rho(1)$  and  $\mathbf{R}(0)$  gets the “banana-shape,” which is shown in Fig. 4, left panel. This non-Gaussian shape is mainly caused by the power estimate  $\mathbf{R}(0)$ , which has a PDF similar to a  $\chi^2$  distribution. By taking the logarithm of  $\mathbf{R}(0)$ , the PDF will be closer to a Gaussian distribution, and the result of this operation is shown in Fig. 4, right panel.

### III. STATISTICAL PROPERTIES OF THE NORMALIZED AUTOCORRELATION ESTIMATE

In this section the general case of a 2-D complex Gaussian process  $x(n, m)$  is treated. The autocorrelation function with radial lag  $n$ , and lateral lag  $m$  is estimated as a weighted sum

of the signal product terms.

$$\mathbf{R}(n, m) = \sum_l \sum_k c(l, k) x^*(n_0 + l, m_0 + k) \cdot x(n_0 + l + n, m_0 + k + m). \quad (2)$$

By taking the expected value of each term in (2), it can be verified that this estimator is unbiased, provided that the sum of the weighting coefficients  $c(l, k)$  equals unity. The second-order moments for the set of autocorrelation estimates have been treated in a previous paper [6], and the formulas are referred in Appendix A. The normalized autocorrelation function is estimated by the formula  $\rho(n, m) = [\mathbf{R}(n, m)]/[\mathbf{R}(0, 0)]$ . Although  $\mathbf{R}(n, m)$  has zero bias for all  $(m, n)$ , this is not the case for  $\rho(n, m)$ , due to the division, and the statistical dependency between  $\mathbf{R}(n, m)$  and  $\mathbf{R}(0, 0)$ . By substituting the division with a second-order linearization, the bias and covariance can be expressed by the covariance of  $\{\mathbf{R}(n, m)\}_{m=0, 1, \dots}$ . The covariance between  $\log[\mathbf{R}(0, 0)]$  and  $\rho(n, m)$  is found by first-order linearization of  $\log[\mathbf{R}(0, 0)]$  around the point  $\log[\mathbf{R}(0, 0)]$ . More details can be found in Appendix A.

$$\begin{aligned} \text{bias}[\rho(n, m)] &\approx -\frac{C(0, n, 0, m) - \rho(n, m)C_*(0, 0, 0, 0)}{R(0, 0)^2} \\ \text{cov}\{\log[\mathbf{R}(0, 0)], \rho(n, m)\} &\approx \frac{C(0, n, 0, m) - \rho(n, m)C_*(0, 0, 0, 0)}{R(0, 0)^2} \\ \text{cov}[\rho(n_1, m_1), \rho(n_2, m_2)] &\approx \frac{C_{12} - \rho_2 C_{01} - \rho_1 C_{02} + \rho_1 \rho_2 C_{00}}{R(0, 0)^2} \\ \text{cov}[\rho(n_1, m_1), \rho(n_2, m_2)^*] &\approx \frac{C_{*12} - \rho_2^* C_{01} - \rho_1 C_{*02} + \rho_1 \rho_2^* C_{00}}{R(0, 0)^2}. \end{aligned} \quad (3)$$

Notation conventions:

$$\begin{aligned} \rho_1 &\equiv \rho(n_1, m_1); \\ \rho_2 &\equiv \rho(n_2, m_2) \\ C_{ij} &\equiv C(n_i, n_j, m_i, m_j) \\ &\equiv \text{Cov}[\mathbf{R}(n_i, m_i), \mathbf{R}(n_j, m_j)] \\ C_{*ij} &\equiv C_*(n_i, n_j, m_i, m_j) \\ &\equiv \text{Cov}[\mathbf{R}^*(n_i, m_i), \mathbf{R}(n_j, m_j)]; \quad i, j = 0, 1, 2. \end{aligned}$$

$n_1$  and  $n_2$  are arbitrary lags,  $n_0 = m_0 = 0$ .

*Example:* The first- and second-order moments of the 3-D estimate  $(x, y, z) = \{\text{Re}[\rho(0, m)], \text{Im}[\rho(0, m)], \log[\mathbf{R}(0, 0)]\}$  are worked out in detail for a signal with angular center frequency  $\omega_1 = \pi$ , with additive, high-pass filtered noise. The total signal including noise has symmetric Doppler spectrum, and hence the expectation value of  $\rho(0, m)$  is real valued for all  $m$ , and the covariance's  $\text{cov}(x, y) = \text{cov}(y, z) = 0$ . The nonzero first- and second-order moments are

$$\begin{aligned} \langle x \rangle &= \rho(n, m) \left[ 1 - \frac{C(0, n, 0, m)}{R(0, 0)R(0, m)} - \frac{C(0, 0, 0, 0)}{R(0, 0)^2} \right] \\ \langle y \rangle &= 0, \quad \langle z \rangle \approx \log(S + N_0) \end{aligned}$$

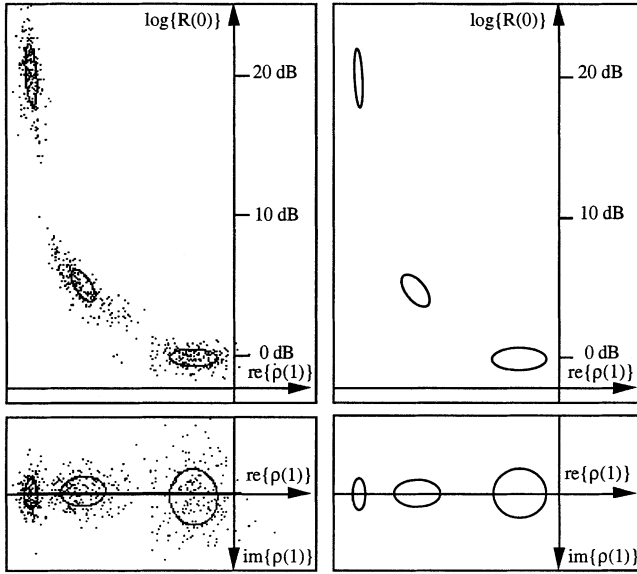


Fig. 5. Two projections ( $x, z$ ) and ( $x, y$ ) of the 3-D probability distribution of  $(x, y, z) = [\rho(0, 1)]$ ,  $\log [R(0)]$ , for signal in noise with SNR 20 dB, 3 dB, and  $-\infty$  dB. To the left simulation results are shown, and to the right are the corresponding values calculated from (5).

$$\begin{aligned} \sigma_x^2 &= \frac{(1 + 2\rho(0, m)^2)C(0, 0, 0, 0)}{2R(0, 0)^2} \\ &\quad - \frac{4\rho(0, m)C(0, 0, 0, m) + C(0, 0, m, m)}{2R(0, 0)^2} \\ \sigma_y^2 &= \frac{C(0, 0, 0, 0) - C(0, 0, m, m)}{2R(0, 0)^2} \\ \sigma_z^2 &= C(0, 0, 0, 0) \\ \rho_{xz} &= \frac{C(0, 0, 0, m) - \rho(0, m)C(0, 0, 0, 0)}{R(0, 0)^2}. \end{aligned} \quad (4)$$

Equation (4) gives a full second-order characterization of the 3-D estimator  $(x, y, z) = [\rho(0, m)]$ ,  $\log [R(0, 0)]$ , for any lag  $m$ . To check the validity of the approximations which lead to (4), the results are compared with computer simulations for some typical signal spectra. The test signals are generated as described in Section II, with three different signal to noise ratios. The output of the estimators are shown in Fig. 5 as scatter plots in the ( $x, y$ ) plane and the ( $x, z$ ) plane.

The variances  $\sigma_1^2$ ,  $\sigma_2^2$  and the correlation coefficient  $\rho$  were calculated in each projection ( $x_1, x_2$ ), and the results indicated with an ellipse

$$\begin{aligned} \left( \frac{x_1 - \langle x_1 \rangle}{\sigma_1} \right)^2 + 2\rho \frac{x_1 - \langle x_1 \rangle}{\sigma_1} \frac{x_2 - \langle x_2 \rangle}{\sigma_2} \\ + \left( \frac{x_2 - \langle x_2 \rangle}{\sigma_2} \right)^2 = (1 - \rho^2) \end{aligned} \quad (5)$$

which is the contour  $p(x_1, x_2) = e^{-1/2}p(\langle x_1 \rangle, \langle x_2 \rangle)$  in the corresponding 2-D Gaussian probability distribution. In Fig. 5 the ellipses in the left panel is given by the simulation results, whereas the ellipses in the right panel is calculated from (4). Numerical results are listed in Table I, both from the computer simulations, and the corresponding values calculated from (4).

The 3-D joint probability function can be used in classification of a color flow image into regions with different

TABLE I  
FIRST- AND SECOND-ORDER MOMENTS OF  $(x, y, z) = [\rho(1)]$ ,  $\log [R(0)]$ . CENTER FREQUENCY  $\omega_1 = \pi$ , WHICH MAKES THE CORRELATION COEFFICIENTS  $\rho_{xy}$  AND  $\rho_{yz}$  VANISH. AVERAGING FILTER LENGTH  $M = 32$ , TRANSIT TIME  $T_t = 8$ , HIGH-PASS FILTER CUTOFF FREQUENCY  $\omega_0 = 0.65$

#### Moments for $(x, y, z)$

	noise only		S/N= 3dB		S/N = 20 dB	
	sim.	calc.	sim.	calc.	sim.	calc.
$\sigma_x$	0.114	0.130	0.106	0.108	0.030	0.025
$\sigma_y$	0.136	0.115	0.072	0.067	0.073	0.073
$\sigma_z$	0.618	0.768	1.641	1.516	2.267	2.088
$\rho_{xz}$	0.062	-0.000	-0.843	-0.799	-0.401	-0.354
$\langle x \rangle$	-0.191	-0.193	-0.719	-0.685	-0.967	-0.965
$\langle z \rangle$	-0.230	0.000	4.977	4.771	20.147	20.043

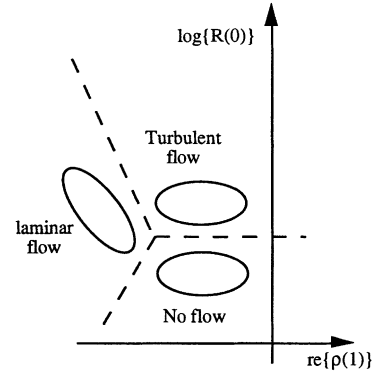


Fig. 6. An illustration of the joint PDF of  $(x, z)$  for three different regions in a color flow image.

characteristic flow patterns. In Fig. 6 the joint PDF is shown for three different flow regions; one with laminar flow giving low bandwidth, one with turbulent flow and high bandwidth, and the third with only noise.

#### IV. PROBABILITY DISTRIBUTION OF THE CORRELATION ANGLE ESTIMATE

The correlation phase angle estimate, defined as  $\phi(n, m) = \arg [R(n, m)]$ , is frequently used as a center frequency estimator. Approximate expression for the variance of this estimator can be found in [5], [8], under the assumption of low fractional variance of  $R(n, m)$ . Time domain expression for the variance have been derived in [4], and the result is generalized in [6] to include the covariance of the set of correlation angle estimators  $\{\phi(n, m)\}$  with arbitrary lag in radial and temporal direction:

$$\begin{aligned} \text{covar} \{ \phi(n_1, m_1), \phi(n_2, m_2) \} \\ \approx \frac{1}{2} \text{Re} \left\{ \frac{C * (n_1, n_2, m_1, m_2)}{R(n_1, m_1) * R(n_2, m_2)} \right. \\ \left. - \frac{C(n_1, n_2, m_1, m_2)}{R(n_1, m_1)R(n_2, m_2)} \right\}. \end{aligned} \quad (6)$$

More detailed statistical analysis of the correlation angle estimator is done by Zrnić [5, pp. 118]. He developed expressions for the probability distribution function (PDF) of the estimator, assuming that the real and imaginary part of the complex autocorrelation estimate  $\mathbf{R}(0, 1)$  are jointly Gaussian random variables. However, for short smoothing filters, which are commonly used in color flow imaging, the PDF of  $R(n, m)$  differs much from a Gaussian form, (see Fig. 1). On the contrary, the normalized correlation estimate  $\rho(n, m)$  has a PDF much closer to the Gaussian form, and (4) gives the first- and second-order moments, which has been shown to match well with simulation results. Since the signal power  $\mathbf{R}(0, 0)$  is real valued and greater than zero, the phase of  $\mathbf{R}(n, m)$  and  $\rho(n, m)$  coincide, and the PDF of the phase angle can be expressed by the first- and second-order moments of  $\rho(n, m)$ . A closed form expression for the phase angle PDF is derived below, under the assumption of symmetrical Doppler spectrum.

Without loss of generality the center frequency is assumed to be zero in the following. When the Doppler spectrum is symmetric with zero center frequency, the real and imaginary parts of  $\rho(n, m)$  are uncorrelated, and the mean value is real valued. The distribution of  $(x, y) = \rho(n, m)$  is then characterized by the three real valued parameters  $\langle x \rangle$ ,  $\sigma_x$ , and  $\sigma_y$ , which are given in (4). This leads to the following expression for the PDF of the phase angle estimator  $\phi = \arg[\rho(n, m)]$  (see Appendix B):

$$\begin{aligned}
 p(\phi) &= \frac{\sigma_1^3 \gamma^2}{2\pi \sigma_2 \cos^2(\phi)} e^{-1/2\sigma_1^2} \\
 &\quad \cdot \{1 + \sqrt{2\pi} \operatorname{erfc}(-\gamma) \gamma e^{\gamma^2/2}\}, \\
 \gamma &= \frac{\cos \phi}{\sigma_1} \left[ \left( \frac{\cos \phi}{\sigma_1} \right)^2 + \left( \frac{\sin \phi}{\sigma_2} \right)^2 \right]^{-1/2}, \\
 \sigma_1 &= \frac{\sigma_x}{\langle x \rangle}, \\
 \sigma_2 &= \frac{\sigma_y}{\langle x \rangle} \\
 \operatorname{erfc}(u) &\equiv \int_u^\infty dv e^{-v^2/2}.
 \end{aligned} \tag{7}$$

This result is compared to computer simulations in Fig. 7, for a complex Gaussian signal in white noise, with two different SNR ( $-6$  dB, and  $0$  dB). The signal is generated as described in Section II, the rms bandwidth is  $0.06\pi$ , and smoothing filter length is 16. Simulations has been performed on data sequences of 50 000 samples.

By numerical integration, the variance of the phase angle estimate has been calculated, using (7). In Fig. 8 the standard deviation is plotted as a function of signal bandwidth, compared to the analytical expression of phase angle variance in (6). It turns out that the results coincide when the total bandwidth of the signal including noise is fairly low, even for short smoothing filter length. This corresponds to a PDF for  $\rho(n, m)$  which is concentrated in a region away from the origin in the complex plane. When the SNR decreases, the PDF of  $\rho(n, m)$  moves toward the origin, and the phase angle distribution gets large side lobes. In this case the values obtained from (6) underestimates the variance, especially for

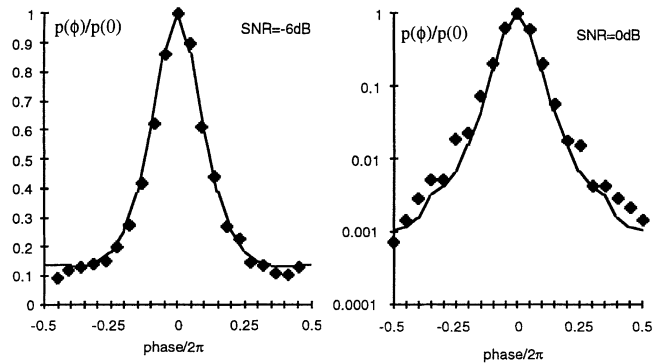


Fig. 7. Probability density for the phase of  $\rho(0, 1)$  for SNR =  $-6$  dB to the left, and SNR =  $0$  dB to the right. The black dots are simulation results. Note that the left figure has linear scale, whereas the right figure has logarithmic scale on the vertical axis.

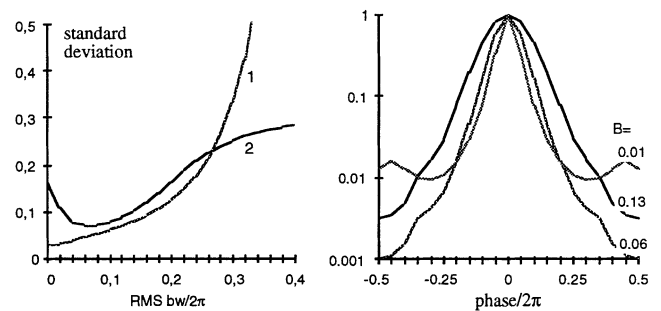


Fig. 8. Standard deviation of the phase angle estimate as a function of bandwidth, using (6) (curve 1), compared with the results obtained from numeric integration using PDF in (7) (curve 2). To the right are curves of the PDF for  $B = 0.01, 0.06$ , and  $0.13$ . The signal has a Gaussian spectrum with white noise, SNR =  $0$  dB, and the averaging filter length  $M = 16$ .

low bandwidth signals. The two methods are compared in Fig. 8 which shows the standard deviation as a function of signal bandwidth, with a SNR of  $0$  dB, and an averaging filter length  $M = 16$ . Curve 1 in the left panel is calculated from (6), and shows a monotone increasing dependency on bandwidth. Curve 2 is calculated from the PDF of (7), and shows a nonmonotone dependency on bandwidth, with a minimum at  $B = 0.06\pi$ . This effect was observed with computer simulated data by Zrnić [5], which shows a dependency on bandwidth which matches well with curve 2, Fig. 8. In the right panel, the PDF for three selected bandwidth values are shown. The main-lobe width decreases with decreasing bandwidth, whereas the side lobes become excessive for low bandwidth, giving an increased variance. For better signal to noise ratio, the nonmonotone relation between the signal bandwidth and estimator standard deviation disappears, as illustrated in Fig. 9.

The effect of radial averaging on the variance of the autocorrelation estimates has been studied in an earlier paper [6]. When the radial sampling rate equals the transmitted pulse-length, the variance reduction was shown to be approximately proportional to the averaging filter bandwidth. In Fig. 10, the effect of radial averaging on the phase angle estimator performance is demonstrated. The reduction in variance due to radial averaging is larger than the decrease in averaging filter bandwidth, especially when the signal bandwidth is low. In this example the standard deviation is reduced by a factor varying from 4 to 2 due to 3 point radial averaging when the

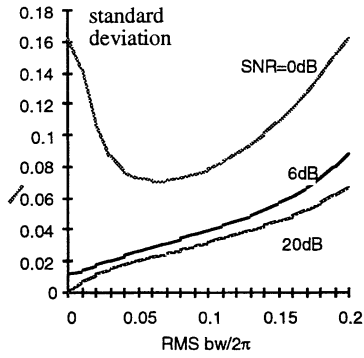


Fig. 9. Standard deviation of the phase estimate as a function of bandwidth for three different SNR, 0 dB, 6 dB, and 20 dB. The signal has a Gaussian spectrum with white noise, and the smoothing filter length  $M = 16$ .

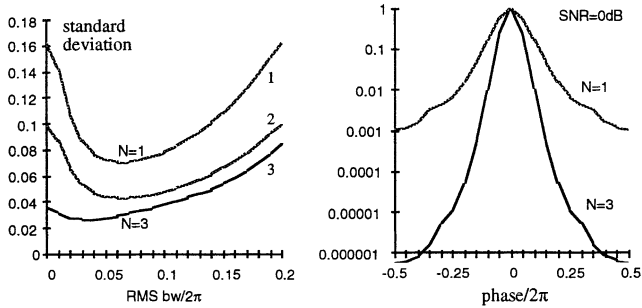


Fig. 10. The effect of radial averaging on the phase angle distribution. To the left: Standard deviation as a function of rms-bandwidth  $B$ . To the right: Phase angle probability density distribution for  $B = 0.06$ . The lower curves are with 3 point radial averaging filter, and the upper are without radial averaging. The middle curve to the left shows the effect of 3 point radial averaging of the angle estimate. Signal to noise ratio SNR = 0 dB, and the temporal averaging  $M = 16$ .

rms signal bandwidth is lower than 0.2. A similar averaging applied after calculating the phase angle is included in Fig. 10, showing a significantly lower variance reduction.

## V. DISCUSSION AND CONCLUSION

The joint probability density function for the estimates  $\rho(0, 1)$ , and  $\log[R(0, 0)]$  has been shown to fit fairly close to a 3-dimensional Gaussian probability distribution for some typical examples of Doppler spectra. Estimated values for the first and second moments showed good agreement with the analytical expressions developed in Section III. This gives a parametric model of the joint PDF, where the parameters are given by the spectral signal properties, as outlined in (5). The parametric model can be used to design optimum color display schemes, with enhanced contrast between different types of blood flow patterns.

The results have been used here to find a more accurate form of the PDF of the correlation angle estimator. Variance calculated from this result shows a nonlinear dependency of bandwidth, which is in agreement with the simulation results presented by Zrni'c [5]. Radial averaging was shown to have a large influence on the phase angle estimator variance. For low signal bandwidth, and low SNR the variance was reduced 16 times with 3 point radial averaging. The same averaging filter applied *after* the mean frequency estimator will reduce the variance at most 3 times. At higher bandwidth, the variance reduction is less pronounced, but still significantly higher than

3. This effect can be explained as follows: As long as the fractional variance of the complex estimator  $\rho(n, m)$  is small, the phase angle distribution will be fairly concentrated around its mean value. When the fractional variance of  $\rho(n, m)$  approaches 1, the phase angle estimate will be spread over the whole interval  $(0 \cdots 2\pi)$ , and its variance will increase faster than the variance of  $\rho(n, m)$ .

A practical consequence of this result is that spatial averaging should be applied to the autocorrelation estimates, and not to the derived signal parameters like the mean frequency, in order to achieve maximum variance reduction.

## APPENDIX A

### COVARIANCE EXPRESSIONS FOR THE NORMALIZED AUTOCORRELATION ESTIMATES, (3)

In this section formulas for the first- and second-order moments for the normalized autocorrelation estimates are developed. The covariance between the complex autocorrelation estimates, as defined in (2) are treated in an earlier paper [6], and is given by

$$\begin{aligned}
 & C_*(n_1, n_2, m_1, m_2) \\
 &= \sum_{kl} c_2(l, k) R(l, k) R^*(l + n_1 - n_2, k + m_1 - m_2) \\
 & C(n_1, n_2, m_1, m_2) \\
 &= \sum_{kl} c_2(l, k) R(l + n_1, k + m_1) R^*(l - n_2, k - m_2) \\
 & c_2(l, k) \\
 &= \sum_{k_1 l_1} c(l_1, k_1) c(l_1 + l, k_1 + k) \\
 & C_*(n_1, n_2, m_1, m_2) \\
 &= \text{Cov} [\mathbf{R}^*(n_1, m_1), \mathbf{R}(n_2, m_2)] \\
 & C(n_1, n_2, m_1, m_2) \\
 &= \text{Cov} [\mathbf{R}(n_1, m_1), \mathbf{R}(n_2, m_2)]. \tag{A1}
 \end{aligned}$$

Without loss of generality, the signal power  $R(0, 0)$  is assumed to equal 1 in the following. The zero mean stochastic variables  $r_{nm}$ ,  $m = 0, 1, \dots$  are defined as

$$\begin{aligned}
 r_{nm} &= \mathbf{R}(n, m) - R(n, m) \\
 \mathbf{R}(n, m) &= R(n, m)(1 + r_{nm}).
 \end{aligned}$$

The second-order moments of  $r_{nm}$  are

$$\begin{aligned}
 \langle r_{n_1 m_1} r_{n_2 m_2} \rangle &= \frac{C(n_1, n_2, m_1, m_2)}{\rho(n_1, m_1) \rho(n_2, m_2)} \\
 \langle r_{n_1 m_1} r_{n_2 m_2}^* \rangle &= \frac{C^*(n_1, n_2, m_1, m_2)}{\rho(n_1, m_1) \rho(n_2, m_2)^*}.
 \end{aligned}$$

Linearizing  $\rho(n, m)$  to second-order, and  $\log[\mathbf{R}(0, 0)]$  to first-order yields

$$\begin{aligned}
 \rho(n, m) &= \frac{R(n, m)(1 + r_{nm})}{R(0, 0)(1 + r_{00})} \\
 &\approx \rho(n, m)(1 + r_{nm})(1 - r_{00} + r_{00}^2) \\
 &\approx \rho(n, m)(1 + r_{nm} - r_{00} - r_{nm}r_{00} + r_{00}^2) \\
 \log[\mathbf{R}(0, 0)] &\approx \log[R(0, 0)] + r_{00}.
 \end{aligned}$$

The bias of  $\rho(n, m)$  is then

$$\begin{aligned} \text{bias}[\rho(n, m)] &\approx \rho(n, m) \\ &\cdot \{ \langle r_{nm} \rangle - \langle r_{00} \rangle + \langle r_{00}^2 \rangle - \langle r_{nm} r_{00} \rangle \} \\ &= -C(0, n, 0, m) + \rho(n, m)C^*(0, 0, 0, 0). \end{aligned}$$

Using first-order linearization, the covariance terms are

$$\begin{aligned} \text{cov} \{ \log [\mathbf{R}(0, 0)], \rho(n, m) \} \\ &= \langle r_{00} \rho(n, m) (r_{nm} - r_{00}) \rangle \\ &= \rho(n, m) \{ \langle r_{nm} r_{00} \rangle - \langle r_{00}^2 \rangle \} \\ &= C(0, n, 0, m) - \rho(n, m)C^*(0, 0, 0, 0). \end{aligned}$$

To simplify notation,  $\rho_1 = \rho(n_1, m_1)$ , and  $\rho_2 = \rho(n_2, m_2)$

$$\begin{aligned} \text{cov} [\rho(n_1, m_1), \rho(n_2, m_2)] \\ &= \rho_1 \rho_2 \{ \langle r_{n_1 m_1} (r_{n_2 m_2} - r_{00} - r_{n_1 m_1} r_{00} + r_0^2 - \langle r_{00}^2 \rangle) \\ &\quad + \langle r_{n_1 m_1} r_{00} \rangle (r_{n_2 m_2} - r_{00} - r_{n_2 m_2} r_{00} \\ &\quad + r_0^2 - \langle r_{00}^2 \rangle + \langle r_{n_2 m_2} r_{00} \rangle) \} \\ &\approx \rho_1 \rho_2 \{ \langle r_{n_1 m_1} r_{n_2 m_2} - r_{n_1 m_1} r_0 - r_0 r_{n_2 m_2} + r_0^2 \\ &\quad + (r_0^2 - r_{n_1 m_1} r_0) (-\langle r_0^2 \rangle + \langle r_{n_2 m_2} r_0 \rangle) \\ &\quad + (r_0^2 - r_{n_2 m_2} r_0) (-\langle r_0^2 \rangle + \langle r_{n_1 m_1} r_0 \rangle) \} \\ &= C(n_1, n_2, m_1, m_2) - \rho_2 C(0, n_1, 0, m_1) \\ &\quad - \rho_1 C(0, n_2, 0, m_2) + \rho_1 \rho_2 C(0, 0, 0, 0) \\ &= C_{12} - \rho_2 C_{01} - \rho_1 C_{02} + \rho_1 \rho_2 C_{00} \\ \text{cov} [\rho(n_1, m_1), \rho(n_2, m_2)^*] \\ &= C^*(n_1, n_2, m_1, m_2) - \rho_2^* C(0, n_1, 0, m_1) \\ &\quad - \rho_1 C^*(0, n_2, 0, m_2) + \rho_1 \rho_2^* C(0, 0, 0, 0) \\ &= C_{12}^* - \rho_2^* C_{01} - \rho_1 C_{02}^* + \rho_1 \rho_2^* C_{00}. \end{aligned}$$

## APPENDIX B

### PROBABILITY DENSITY FUNCTION FOR THE CORRELATION ANGLE ESTIMATE

Let  $z = x + iy$  be a complex random variable, where the real and imaginary parts are independent Gaussian random variables with mean values  $\langle x \rangle = 1$ ,  $\langle y \rangle = 0$ , and variances  $\sigma_1^2$ ,  $\sigma_2^2$ . The probability density function for the phase angle of  $z$  is calculated in the following. In polar coordinates  $(r, \phi)$  the PDF for the complex variable  $z = r e^{i\phi}$  has the form

$$p(r, \phi) = cr \exp \left[ -\frac{(r-b)^2}{2\sigma(\phi)^2} \right] \quad (\text{B1})$$

where the parameters  $\sigma(\phi)$ ,  $b$ , and  $c$  are defined as

$$\begin{aligned} \sigma(\phi) &= \left[ \left( \frac{\cos \phi}{\sigma_1} \right)^2 + \left( \frac{\sin \phi}{\sigma_2} \right)^2 \right]^{-1/2} \\ b &= \frac{\sigma(\phi)^2}{\sigma_1^2} \cos(\phi) \\ c &= \frac{1}{2\pi\sigma_1\sigma_2} \\ &\cdot \exp \left\{ -\left[ \frac{1 - \frac{\sigma(\phi)^2}{\sigma_1^2} \cos^2 \phi}{2\sigma_1^2} \right] \right\}. \end{aligned} \quad (\text{B2})$$

The PDF for the phase  $\phi$  is obtained by integration of  $p(r, \phi)$

over  $r$

$$\begin{aligned} p(\phi) &= \int_0^\infty dr p(r, \phi) \\ &= c\sigma^2(\phi) \left\{ \exp \left[ -\frac{\sigma(\phi)^2 \cos^2 \phi}{2\sigma_1^4} \right] \right. \\ &\quad \left. + \frac{\sigma(\phi)}{\sigma_1^2} \cos \phi \sqrt{2\pi} \text{erfc} \left[ -\frac{\sigma(\phi)}{\sigma_1^2} \cos \phi \right] \right\} \quad (\text{B3}) \end{aligned}$$

where the error function  $\text{erfc}$  is defined as

$$\text{erfc}(u) = \int_u^\infty dv e^{-v^2/2}. \quad (\text{B4})$$

Setting  $\gamma = [\sigma(\phi)/\sigma_1^2] \cos \phi$ , gives the final form of the probability function  $p(\phi)$  for the phase angle

$$\begin{aligned} p(\phi) &= \frac{\sigma_1^3 \gamma^2}{2\pi\sigma_2 \cos^2(\phi)} e^{-1/2\sigma_1^2} \left\{ 1 + \sqrt{2\pi} \text{erfc}(-\gamma)\gamma e^{\gamma^2/2} \right\} \\ \gamma &= \frac{\cos \phi}{\sigma_1^2} \left[ \left( \frac{\cos \phi}{\sigma_1} \right)^2 + \left( \frac{\sin \phi}{\sigma_2} \right)^2 \right]^{-1/2}. \end{aligned} \quad (\text{B5})$$

## ACKNOWLEDGMENT

The authors would like to thank A. Heimdal at the Department of Biomedical Engineering, University of Trondheim, for revising the manuscript.

## REFERENCES

- [1] W. R. Brody and J. D. Meindl, "Theoretical analysis of the CW Doppler ultrasonic flowmeter," *IEEE Trans. Biomed. Eng.*, vol. BME-21, pp. 183–192, 1974.
- [2] B. A. J. Angelsen, "A theoretical study of the scattering of ultrasound from blood," *IEEE Trans. Biomed. Eng.*, vol. BME-27, pp. 61–67, 1980.
- [3] C. Kasai, K. Namekawa, A. Koyano, and R. Omoto, "Real-time two-dimensional blood flow imaging using an autocorrelation technique," *IEEE Trans. Sonics Ultras.*, vol. SU-32, pp. 458–464, 1985.
- [4] D. S. Zrni'c, "Spectral moment estimates from correlated pulsed pair," *IEEE Trans. Aerosp. Electron.*, vol. AES-13, pp. 344–354, 1977.
- [5] ———, "Estimation of spectral moments for weather echoes," *IEEE Trans. Geosci. Electron.*, vol. GE-17, pp. 113–128, 1979.
- [6] H. Torp, K. Kristoffersen, and B. Angelsen, "Autocorrelation techniques in color flow imaging. Signal model and statistical properties of the autocorrelation estimates," *IEEE Trans. Ultrason., Ferroelec., Frequency Contr.* vol. 41, pp. 604–612, 1994.
- [7] K. Aggarwal, E. Philpot, and N. Nanda, "Understanding different types of color Doppler systems," in *Textbook of Color Doppler Echocardiography*, N. Nanda, Ed. Philadelphia, PA: Lea & Febiger, 1989, pp. 74–98.
- [8] K. Kristoffersen, "Time domain estimation of the center frequency and spread of Doppler spectra in Doppler ultrasound," *IEEE Trans. Ultrason., Ferroelec., Freq. Contr.* vol. 35, pp. 484–497, 1988.

**Hans Torp** (M'92) was born in Sarpsborg, Norway, in 1953. He received the M.S. and Dr.Techn. degrees from the University of Trondheim, Norway, in 1978 and 1992, respectively.

From 1979 to 1983 he was with the Division of Automatic Control, SINTEF (The foundation of Scientific and Industrial Research) in Trondheim. Since 1983 he has been with the Department of Biomedical Engineering, Faculty of Medicine, University of Trondheim. He is currently a research fellow, holding a stipend from the Norwegian Research Council. His research areas includes stochastic signal/image processing with applications in ultrasonic imaging, Doppler and color flow imaging.

**Kjell Kristoffersen** was born in Karmøy, Norway, in 1952. He received the M.S. and Dr. Techn. degrees from the Norwegian Institute of Technology, Trondheim, Norway in 1978 and 1986, respectively.

From 1978 to 1984 he worked with research and development in several areas of process identification and Doppler ultrasound at the Division of Automatic Control, SINTEF, Trondheim, Norway. Since 1984 he has been involved with the development of medical ultrasound imaging systems at Vingmed Sound A.S., where he currently holds the position as Director of Research. His research interests include signal processing with application to medical imaging and noninvasive diagnosis.

**Bjørn A. J. Angelsen** (M'79–SM'82) was born in Vestvågøy, Norway, in 1946. He received the M.S. and Dr. Techn. degrees from the Norwegian Institute of Technology, Trondheim, Norway, in 1971 and 1977, respectively.

From 1971 to 1972 he worked on infrared detectors at the Norwegian Defence Research Establishment, Kjeller, Norway. From 1972 to 1975 he held a stipend at the Norwegian Institute of Technology and from 1975 to 1982 he was with the Division of Control Engineering, SINTEF (The Foundation of Scientific and Industrial Research, Norwegian Institute of Technology) Trondheim, Norway. From 1977 to 1978 he was on leave at the Department of Electrical Engineering, University of California, Berkeley, and the Division of Biomedical Engineering, Stanford Research Institute, Menlo Park, CA. Since 1980 he has been Adjunct Professor of Biocybernetics and since 1983 a Professor of Biomedical Engineering at the University of Trondheim. His research interests include noninvasive diagnosis with emphasis on ultrasonic diagnosis.